Proceedings of the
Annual Stability Conference
Structural Stability Research Council
St. Louis, Missouri, April 2-5, 2019

On the interaction between local and lateral-torsional buckling of I-shaped slender section beams

Carlos Couto[1], Paulo Vila Real[2]

Abstract
The work presented herein addresses the effect of local buckling on the carrying capacity of I-shaped beams with slender sections and its interaction with the lateral-torsional buckling failure mode. The use of slender I-shaped sections is particularly attractive for long-span beams where the designer profits from the bending resistance of the flanges while optimizing the web dimensions up to an extent where its main function is to provide efficient support to the flanges. However, since limited research has been undertaken on this subject, not only the safety level of existing design standards is unclear but also the influence of residual stresses, plate imperfections and global imperfections has not yet been consistently addressed for such cases. The paper studies such influence by employing material and geometrical nonlinear, shell-element based FE analysis. Different assumptions are considered in terms of the magnitude of the geometrical imperfections and distribution of residual stresses on the numerical models and the results are compared with the North American design code, AISC360-16, and the European design code, Eurocode 3. Based on the implicit assumptions of the design codes, it was found that AISC360-16 provides an upper limit for the beam's resistance and the Eurocode 3 a lower bound, mainly because residual stresses have a strong impact in the carrying capacity of the beams with slender section. This expands the observations of other authors in the context of studies of beams with non-slender sections. Hence, it is recommended that the proper characterization of these material imperfections is addressed in the future on the basis of experimental tests and, if necessary, that amendments are made to the design codes.

1. Introduction

For slender sections beams, owing to the high width-to-thickness ratio of the plates, local buckling may reduce the ultimate strength and, as a consequence, the load-carrying capacity of the steel beams (Basler and Thürlimann, 1960). At the same time, due to its nature, local buckling is generally considered in the design codes as local phenomena and it is accounted for at the cross-section level which, in a certain way, provide an uncoupled approach to this interaction problem. For example, in the AISC360 (AISC, 2016), the member design for flexure of I-shaped sections (chapters F) depends upon the section classification for local buckling (section B4.1). If a section has a slender web, then chapter F5 applies. Thus, if section limits are not well defined it may lead

[1] Post-doc Research Student, RISCO - University of Aveiro, Portugal <ccouto@ua.pt>
[2] Full Professor, RISCO - University of Aveiro, Portugal, <pvreal@ua.pt>

to inaccurate procedures. Subramanian and White (2017a), for example, propose improvements to the AISC360-16, for the noncompact web-slenderness limit. According to the Eurocode 3 (CEN, 2005), the section classification is also necessary and, if a section is slender – Class 4 according to Eurocode 3, a reduced (or effective) section needs to be considered and calculated according to Part 1-5 (CEN, 2006) to account for the local buckling, and later used in the member in the bending verification procedures (Clause 6.3.2, see also (Rebelo *et al.*, 2009; Simões da Silva *et al.*, 2009)). However, previous research by Schillo *et al.* (2018) and Couto and Vila Real (2019) found that the effective width method in Part 1-5 might overestimate the section capacity in compression. Since the same expressions are used for flexure, differing only on the stress distribution considered on the web, the same limitations are expected.
In addition, within the scope of the Eurocode 3, it was previously demonstrated that the local-global interaction could be better accounted for trough the inclusion in the design procedures of an Effective Section Factor, that was developed by the authors for the case of fire (Couto *et al.*, 2016, 2018) and also observed in a numerical study at normal temperature (Couto *et al.*, 2015), but this study did not cover different assumptions of residual stress distributions and/or geometrical imperfections. In fact, various researchers noticed that the use of nominal residual stresses and imperfections in the Finite Element studies resulted in lower capacity prediction when compared to experimental tests (Subramanian and White, 2017b, 2017c). The issue of the geometrical imperfections and residual stresses to use in the numerical models is of great importance. In fact, over conservative assumptions may lead to unnecessary lower predictions in comparison to real test cases but, on the other hand, as more and more design codes rely substantially on numerical calibrated results, the underestimation of the effects of imperfections could produce unsafe design predictions. Although the variability of these parameters in the strength curves for LTB has been investigated by Subramanian and White (2017c), in the present paper such variability is analyzed for cases where the local-global interaction is more preeminent.

2. Brief overview of North American and European design codes

2.1. AISC360-16

This section intends to briefly address the design philosophy of the North American design code AISC360 (AISC, 2016), more particularly the chapter F5 regarding the flexural design of slender web sections. According to this clause, the Compression Flange Yielding, Lateral-Torsional Buckling, Compression Flange Local Buckling and the Tension Flange Yielding (only for monosymmetric cross-sections) limit states should be checked.
For the Compression Flange Yielding limit state, the nominal flexural strength is calculated as,

$$M_n = R_{pg} F_y S_{xc} \tag{1}$$

where F_y is the steel yield stress, S_{xc} corresponds to the elastic section modulus referred to compression flange and R_{pg} is the bending strength reduction factor given by:

$$R_{pg} = 1 - \frac{a_w}{1200 + 300 a_w}\left(\frac{h_c}{t_w} - 5.7\sqrt{\frac{E}{F_y}}\right) \tag{2}$$

where for doubly-symmetric sections h_c corresponds to the web clear depth, and a_w is calculated as,

$$a_w = \frac{h_c t_w}{b_{fc} t_{fc}} \tag{3}$$

with t_w being the web thickness and b_{fc} and t_{fc} being respectively the compression flange width and thickness.
For the lateral-torsional buckling (LTB) limit state, F_y is replaced by F_{cr} that is calculated based on the unbraced length L_b and its relation to the so-called "plastic" anchor point L_p and the "slender" anchor point L_r. Thus, for the LTB limit state, the nominal flexural strength M_n is given by,

$$M_n = R_{pg} F_{cr} S_{xc}. \tag{4}$$

For $L_b \le L_p$, the limit states does not apply, and for $L_p < L_b \le L_r$ the critical stress F_{cr} is calculated as,

$$F_{cr} = C_b \left[F_y - \left(0.3 F_y\right)\left(\frac{L_b - L_p}{L_r - L_p} \right) \right] \le F_y \tag{5}$$

and when $L_b > L_r$, the critical stress F_{cr} is calculated as

$$F_{cr} = \frac{C_b \pi^2 E}{\left(\frac{L_b}{r_t} \right)^2} \le F_y \tag{6}$$

in these equations, C_b is a modification factor to account for nonuniform moment diagrams and r_t is the effective radius of gyration for LTB defined as:

$$r_t = \frac{b_{fc}}{\sqrt{12\left(1 + \frac{1}{6} a_w\right)}} \tag{7}$$

finally, the anchor point lengths are calculated as,

$$L_p = 1.1 r_t \sqrt{\frac{E}{F_y}} \tag{8}$$

and

$$L_r = \pi r_t \sqrt{\frac{E}{0.7F_y}}\,. \tag{9}$$

It is worth mention, however, that for L_p, the AASTHO (2016) recommends the use of 1.0 instead of 1.1 in the Eq. (8). According to AASTHO specification, this limit is based on linear regression analysis within the region corresponding to the inelastic lateral torsional buckling equation for a wide range of data from experimental flexural tests involving uniform major-axis bending and in which the physical effective length for LTB is effectively 1.0. On this matter, Subramanian and White (2015, 2017b) propose even a smaller plateau of 0.63.

Regarding the compression flange local buckling limit state, it is only applied for noncompact or slender flanges. The nominal flexural strength M_n is calculated with Eq. (4) but with F_{cr}, for noncompact flanges, given by,

$$F_{cr} = \left[F_y - \left(0.3F_y\right)\left(\frac{\lambda - \lambda_{pf}}{\lambda_{rf} - \lambda_{pf}} \right) \right] \tag{10}$$

and for slender flanges by,

$$F_{cr} = \frac{0.9Ek_c}{\left(\frac{b_{fc}}{2t_{fc}} \right)} \tag{11}$$

where $k_c = 4/\sqrt{h/t_w}$ but shall not be taken less than 0.35 nor greater than 0.76, $\lambda = b_{fc}/2t_{fc}$, $\lambda_{pf} = \lambda_p$ and $\lambda_{rf} = \lambda_r$ respectively the compact and noncompact limiting slenderness as defined in Table B4.1b of the AISC360-16 norm. Figure 1 shows the buckling curve representation for the I600×4.5+180×tf sections in Table 2

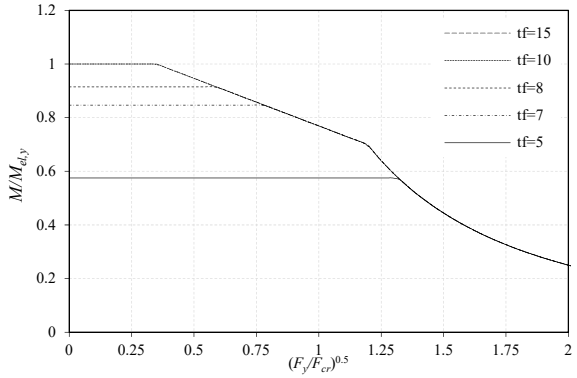

Figure 1: Design curves according to AISC360-16 for the I600×4.5+180×t_f sections in Table 2.

Here, the design curves were normalized by $M_{el,y}$, the elastic flexural capacity of the cross-sections and the results are plotted with F_{cr} calculated with Eq. (6) but without considering the F_y limit.

2.2. Eurocode 3 design formulae for lateral-torsional buckling

According to the present version of EC3, the design buckling resistance moment of a steel member against LTB, $M_{b,Rd}$, is determined by multiplying the design value of the cross-sectional resistance moment M_{Rd} by a reduction factor χ_{LT} that accounts for the effects of this type of buckling coupled with the global imperfections and residual stresses that are present in real members:

$$M_{b,Rd} = \chi_{LT} \cdot M_{Rd} = \chi_{LT} \cdot W_y \cdot \frac{f_y}{\gamma_{M1}} \tag{12}$$

where, for cross-sections of Class 4, the section modulus W_y corresponds to the effective one, $W_{eff,y}$, determined with the effective widths given in clause 4.4 of EN 1993-1-5 (CEN, 2006).

For the determination of the reduction factor for LTB, EC3 presents two different formulae: the "General case" (clause 6.3.2.2) and the "Specific case" (clause 6.3.2.3). These methods are based on an extension to the LTB case of the Ayrton-Perry formulation for flexural buckling, where the first-yield equation of a column with an initial sinusoidal deformation is first obtained by using second-order theory, and then calibrated to numerical and experimental results by introducing an equivalent imperfection factor. γ_{M1} is the partial safety factor, taken as 1.0 in this study.

More particularly, the "General case" (GC) for LTB is identical to the procedure for the column flexural buckling (clause 6.3.1.2 of EC3-1-1), with the reduction factor given by:

$$\chi_{LT} = \frac{1}{\varphi_{LT} + \sqrt{\varphi_{LT}^{\,2} - \overline{\lambda}_{LT}^{\,2}}} \leq 1.0 \tag{13}$$

with

$$\varphi_{LT} = 0.5 \cdot \left[1 + \alpha_{LT} \left(\overline{\lambda}_{LT} - 0.2 \right) + \overline{\lambda}_{LT}^{\,2} \right] \tag{14}$$

and where $\overline{\lambda}_{LT}$ is the normalized slenderness for LTB, given by:

$$\overline{\lambda}_{LT} = \sqrt{\frac{M_{Rd}}{M_{cr}}} \tag{15}$$

M_{cr} is the elastic critical moment obtained numerically or given in the literature based on gross cross-sectional properties and taking into account the loading conditions, the real moment distribution and the lateral restraints.

Finally, the Eurocode 3 defines four buckling curves for LTB based on the depth-to-width ratio h/b for the GC curves are the ones found in Table 1.

Table 1: Recommended LTB design curves for the General Case of Eurocode 3.

Cross-section	Limits	Buckling Curve
Rolled I-sections	$h/b \leq 2$	a
	$h/b > 2$	b
Welded I-sections	$h/b \leq 2$	c
	$h/b > 2$	d
Other cross-sections	-	d

These curves – a,b,c,d – depend on the value of the imperfection α_{LT}, 0.21, 0.34, 0.49 and 0.76 respectively, and are depicted in Figure 2. Accordingly, for the sections in this study, buckling curve "d" is used.

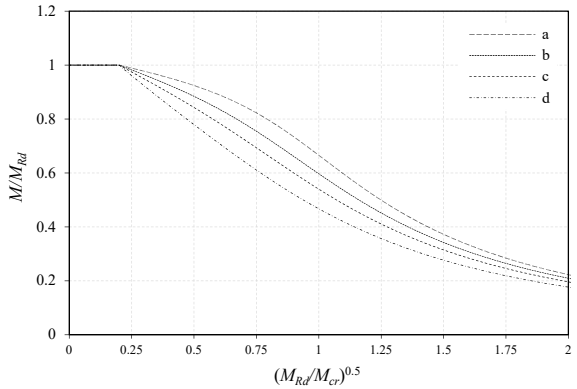

Figure 2: Graphical representation of the buckling curves presented in Eurocode 3 for LTB.

The "Specific Case" is not addressed in this study because it will be replaced in the future revision of the Eurocode 3 with the method developed by Taras and Greiner (2010).

3. Numerical model

The software package SAFIR (Franssen and Gernay, 2017) was used to obtain the numerical results with the Finite Element Method by performing. The formulation of the default shell finite element in SAFIR is detailed in Talamona and Franssen (2005). This shell finite element has six DOF's *per* node (three displacements and three rotations) and the software can perform full geometrical and material non-linear analysis.

Regarding the mesh, after a sensitivity analysis, the flange was modelled with 12 elements, the web with 22 and 100 elements each 10 m were used along the length of the member. Fork-supports were used at both ends of the structural member to prevent the displacements in z-direction and y-direction, to prevent the rigid body movement the displacements in x-direction were constrained at mid-span. The beam was subjected to a constant bending moment by applying end-moments at both ends with equal value and opposite signs by means of nodal forces. Additionally, end-plates were included with a thickness equal to 10 times the web thickness to ensure correct load distribution. The numerical model is shown in Figure 3.

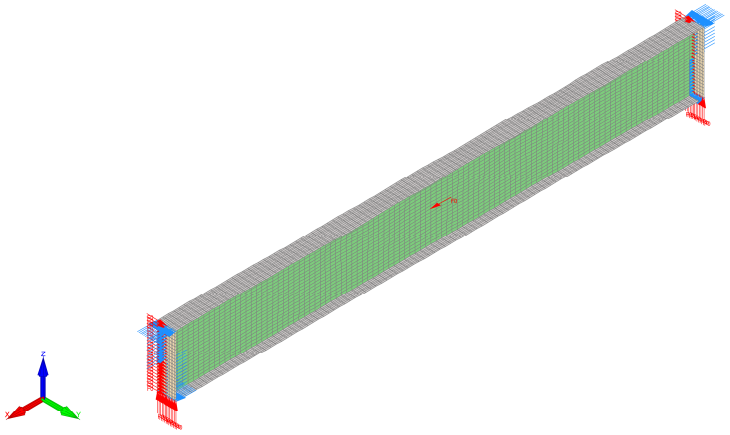

Figure 3: Detail of the numerical model.

Residual stresses and geometrical imperfections were included in the numerical models. For the residual stresses, they were defined as initial state conditions (using the appropriate data file input in SAFIR) consisting on the patterns given in Figure 4.

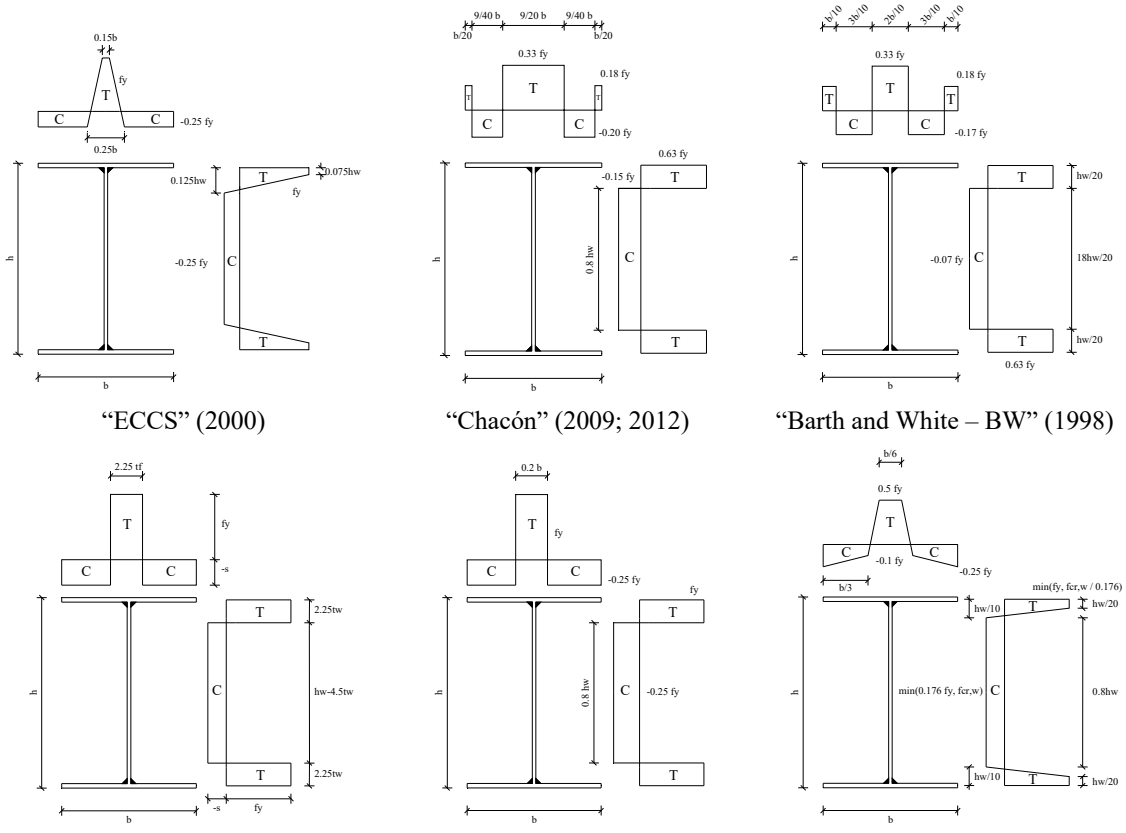

"ECCS" (2000) "Chacón" (2009; 2012) "Barth and White – BW" (1998)

"Clarin" (2004) "Taras" (2010) "Best-fit Prawel" (Kim, 2010)

Figure 4: Pattern of the residual stresses considered in this study for welded profiles.

For the geometrical imperfections, the original node coordinates were displaced to a new position to replicate the shape and amplitude of the desired imperfection. Both local (or plate, see Figure 12) and global (or member, see Figure 5) imperfection's shape are given by a Linear Buckling Analysis (LBA). Because LBA analyses are not possible in SAFIR the software Cast3M (CEA, 2015) was used as an alternative for that purpose.
For the solution of the non-linear equations the Newton-Raphson method was used with 10^{-3} times the plastic flexural capacity of the cross-section applied as the initial load and then increased during the solution process until equilibrium could not be established, thus the ultimate strength corresponds to the last converged loadstep (or maximum load applied) during the analysis.
The steel S355 was considered in this study, with an elasto-plastic stress-strain relationship material law defined by a yield strength of 355 MPa, a Young modulus of 210 GPa and a Poisson ratio of 0.3, for the plasticity criterion the von-Mises yield surface is adopted by default in SAFIR. For the LBA, the yield part of the steel material law was, naturally, omitted. For this analysis, the displacements in y-direction were blocked at the web-flange intersection to force the local modes and for the global modes multi-point constraints were used to constrain the rotation about the longitudinal axis (RotX) of all the nodes in the plane of the cross-section to the rotation (RotX) of the node at the shear center. This numerical model has been extensively used by the authors in previous studies.

4. Cases studied

Table 2 shows the sections that were considered in this study. Different flange classes were chosen as defined in Eurocode 3 and AISC360-16. For the web class, a non-compact section was considered according to the AISC360-16 classification, although this section is Class 4 according to Eurocode 3, which corresponds to the slender classification according to AISC360-16 terminology. In particular, for a web with 600 mm, a web thickness of 4.3 mm would correspond to the slender limit according to AISC360-16 classification, thus the considered section is close to that boundary. Also, although the AASHTO (2016) includes recommendations for the proportion limits of slender sections, these limits were ignored to have a broader scope of analyzed sections. The sections not fulfilling these limits are indicated in the table.

Table 2: Sections analyzed in numerical simulations.

Designation (I $h_w \times t_w + b_{fc} \times t_{fc}$)[1]	Web class AISC360-16	Web class EC3	Flange class AISC360-16	Flange class EC3
I600×4.5+180×15	Non-compact	4	Compact	1
I600×4.5+180×10	Non-compact	4	Non-compact	3
I600×4.5+180×8	Non-compact	4	Non-compact	3
I600×4.5+180×7	Non-compact	4	Non-compact[2]	4
I600×4.5+180×5	Non-compact	4	Slender[2]	4
I850×6+400×30	Slender	4	Compact	1
I850×6+400×20	Slender	4	Compact	3
I850×6+400×18	Slender	4	Non-compact	3
I850×6+400×15	Slender	4	Non-compact[2]	4
I850×6+400×10	Slender	4	Slender[2]	4

1. h_w and t_w are the web height and thickness; b_{fc} and t_{fc} are the flange width and thickness.
2. Flange dimensions do not fulfill proportion limits in AASHTO (2016).

5. Sensitivity to initial imperfections and residual stresses

5.1. Initial global imperfections

The influence of different global imperfection's amplitudes on the load-carrying capacity reduction is investigated here. The objective is to describe this influence for a beam, first with a negligible small global imperfection of L/10000 and then with two sets of global imperfections of L/1000 and L/2000. The shape of the global (or member) imperfection that was included in the numerical simulations is given in Figure 5 (see also §3) and corresponds to the first global eigenmode from a LBA.

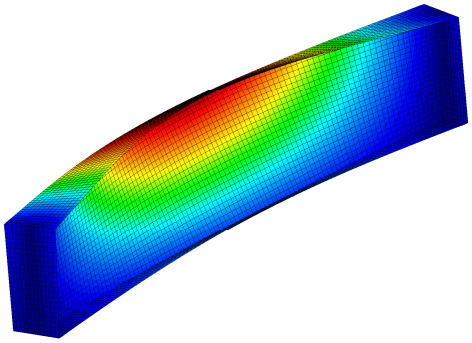

Figure 5: Shape of the global imperfection affine to the deformed geometry of the 1st global eigenmode from a LBA.

Additionally, a very small plate imperfection of 0.1 mm was also included in the simulations in this part of the study. Since the influence of the global imperfections depends also, as demonstrated, on the presence of residual stresses, three cases are investigated in this regard, in a first case they are disregarded (denoted "No Res Stress") and later assumed to have either the "Barth and White" (B&W) pattern or the "ECCS" pattern, which correspond to the minimum and maximum influence on the results, as later described in §5.2.

Results are plotted for the I600×4.5+180×8 cross-section in Figure 6 and Figure 7 in terms of M / M_{Rd} ratio versus the slenderness given by Eq. (15). In this case, M_{Rd} corresponds to the effective section flexural resistance calculated with the effective width expressions given in Part 1-5 of the Eurocode 3 (CEN, 2006).

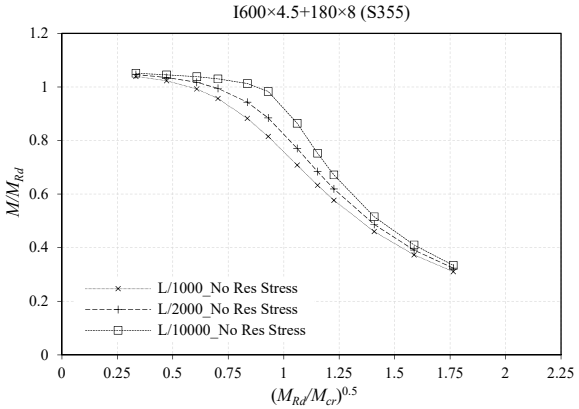

Figure 6: Effect of global imperfection amplitude without residual stresses.

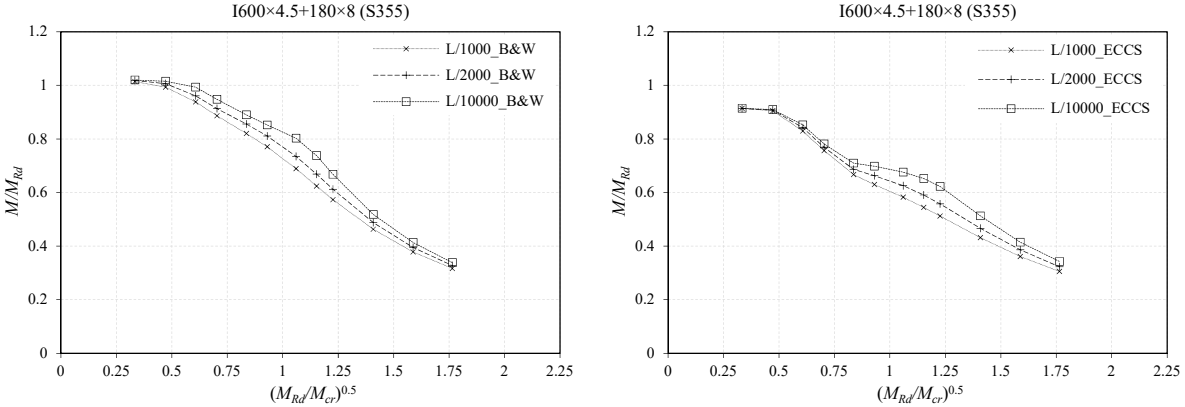

Figure 7: Effect of global imperfection amplitude and "B&W" (left) and "ECCS" (right) residual stress patterns.

The reduction in resistance due to global imperfections is properly shown in Figure 6 where residual stresses were not included. In this case, as it was expected, the reduction in the ultimate strength is proportional to the amplitude of the global imperfections included in the simulations. Until a slenderness of approximately 0.9, the reduction in the capacity is almost negligible for an imperfection of L/10000 but if L/1000 is considered, the decrease in resistance is noticed for a slenderness higher than 0.5. However, when residual stresses are included in the models, the results show that the load-carrying capacity starts to become less sensitive to the amplitude of the imperfections and, more particularly, for the "ECCS" residual stress pattern, until a slenderness of 0.8, the amplitude of the global imperfection has a negligible impact on the resistance. It is evident that, for this slenderness range, the member capacity is governed by the inelastic capacity and that the residual stresses have a stronger influence on this range than for higher values of slenderness where the response of the member is governed by its elastic capacity. The justification for such phenomena lies on the onset of local buckling due to presence of residual stresses and the strong interaction between this two phenomena which affects the carrying capacity of the beams. Although not shown here, the results are similar for all the cross-sections investigated in this paper, thus are not influenced by the possible interaction between the local buckling and the lateral-torsional buckling and, therefore, are likely to be general, for welded sections.

5.2. Residual stresses

This section describes the influence of the residual stresses in the flexural capacity of the slender beams. Residual stresses are unavoidable in the fabrication of steel members, and for built-up girders, those made of welded plates, the numerical results show that these material imperfections have a significant influence on the ultimate strength of the members. It worth mention that, during the development of the European design curves, different curves were defined in order to properly account with the effect of residual stresses while for the American code the attention to this subject has been relegated to minor importance.

To analyze the influence of residual stresses, the simulations were carried out considering an initial global imperfection of different amplitude (L/10000, L/2000 and L/1000) and including different residual stresses distributions in the models, according to Figure 4. Additionally, a small plate imperfection of 0.1 mm was also included in the simulations. The shape of geometrical imperfections is based on the shape of the corresponding eigenmode from a LBA.

Results are shown for two sections in Figure 8 for a global imperfection of L/1000 and in Figure 9 the average results obtained for different global imperfections are also indicated. As before, $\bar{\lambda}_{LT}$ was calculated with M_{Rd} given by the effective width expressions in Part 1-5 of the Eurocode 3.

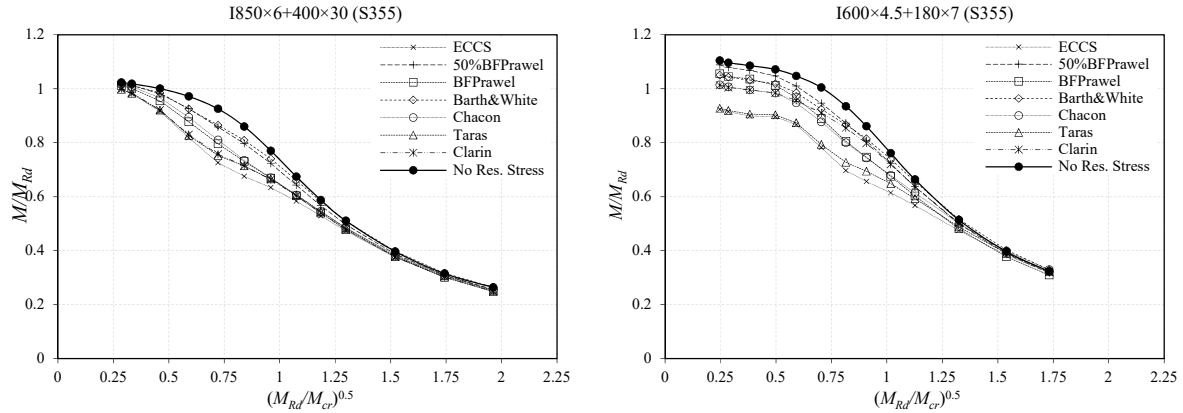

Figure 8: Influence of different residual stresses pattern for the section I850×6+400×30 (left) and I600×4.5+180×7 (right) assuming a global imperfection of L/1000.

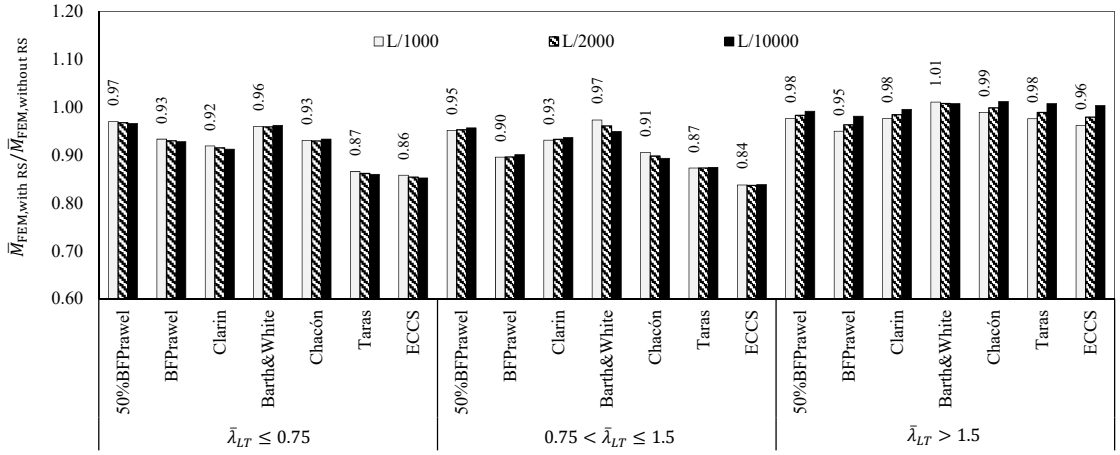

Figure 9: Average results for the influence of different residual stress patterns and global imperfections (numbers in labels are for L/1000 imperfection).

The influence of the residual stresses, as expected, is higher until the slender range (here assumed as $\bar{\lambda}_{LT} \approx 1.5$) and depending on the flange slenderness it affects also the behavior for smaller values of $\bar{\lambda}_{LT}$ as demonstrated for the more slender section in Figure 8b, due to the stronger interaction between local buckling and lateral-torsional buckling for these types of sections.
Regarding the different patterns, considering 50% of the Best-fit Prawel returns similar results as the "Barth&White" pattern and constitute the lower bound for the influence of residual stresses on the girder capacity. On the other hand, the "Taras" and "ECCS" profiles give the maximum reduction in resistance due to the presence of the residual stresses and, thus, constitute the upper bound. Interestingly, the influence of "Clarin" pattern is higher in the 180×30 case because it depends on the thickness, and although f_y is defined in this pattern as the maximum tensile stress, the results are only closer to the "ECCS" and "Taras" profiles for the thicker plates. This shows that not only the magnitude of the residual stresses is of importance but also the distribution of the residual stresses should be properly dissected in order to have consistent results between numerical analysis and the reality. Finally, the influence of residual stresses is insensitive to the amplitude of the global imperfection that was assumed in the finite element simulations.

5.3. Initial plate imperfections

On the plateau range, the capacity of a girder is governed by the section flexural capacity section, and, as the unbraced length increases, the lateral-torsional buckling limit state becomes relevant and after a certain length (L_p – according to the AISC360-16 specification) it may limit the beam capacity. If a section contains thinner plates, the presence of plate imperfections increases the possibility of local buckling to develop and weaken the flexural capacity. Not only the presence of plate imperfections will affect the ultimate strength of a beam, but will also play an important role in the definition of the unbraced length for which the lateral-torsional buckling limit state applies. However, the purpose of this section is to determine the influence of plate imperfections and the evaluation and definition of L_p should be addressed in future studies.
First, the girders with the cross-sections from Table 2 were simulated assuming no residual stresses, a global imperfection of L/1000 and a small plate imperfection of 0.1 mm, which should correspond to a negligible one, and are denoted "G" standing for the global imperfection case. Later, those cases were simulated including plate imperfections, the shape of which was taken from the deformed geometry of a LBA analysis and the maximum amplitude for the plate imperfections considered as $b/100$ or $b/200$, where b corresponds to the width of the flange or the height of the web depending on the most displaced node on the LBA analysis. These cases are denoted "GL" because they contain both global (G) and local/plate imperfections (L). Finally, the simulations were carried out, for each of the previous assumptions with the inclusion of residual stresses. In this case, the "ECCS" and "Barth & White" patterns were included since they represent the most significant and least significant influence of the residual stresses (see §5.2) on the results, these cases being denoted "GLR". Figure 10 plots the buckling curve representation for two sections.

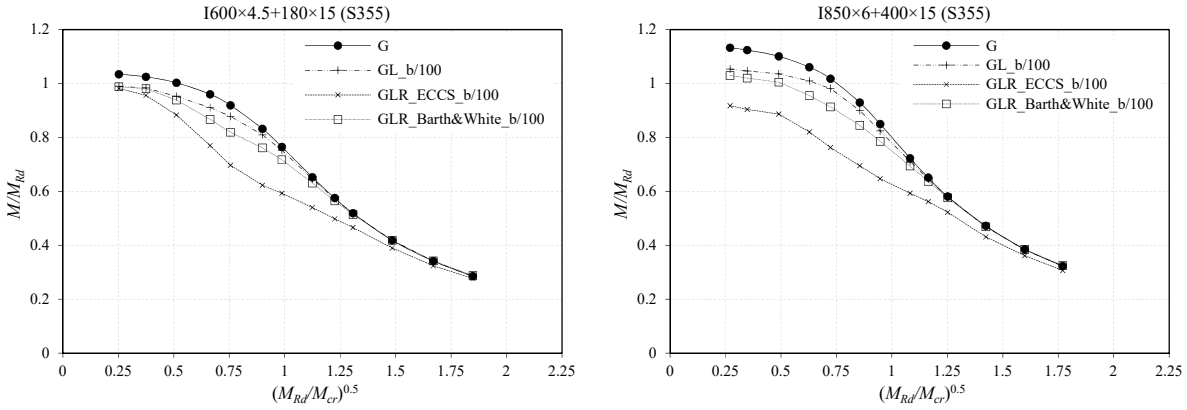

Figure 10: Buckling curve representation of influence of different residual stress patterns for the section I850×4.5+180×15 (left) and I850×6+400×15 (right).

The local imperfections (denoted "L" in the figures) have a detrimental effect on the LTB capacity of the girders. This influence is slightly higher for lower values of the beam slenderness where the load-carrying capacity is mainly governed by the flexural capacity of the cross-section, especially if the section itself contains slender plates (compare the numerical results for global imperfections, the circles, with the ones with global and local imperfections, the plus signs, in Figure 10). This is further illustrated in Figure 11, for the comparison of the ratio between using amplitudes of b/100 and b/200 for the plate imperfections or no plate imperfections. The variation of this ratio suggests that the influence of plate imperfections is different depending on the plate's width-to-thickness ratio on the cross-section, being more relevant for more slender cross-sections and less significant for their counterparts, especially for lower values of the member slenderness. From these results, it is observed that as the member slenderness increases, the influence of the plate imperfections decreases when the resistance becomes governed by the elastic capacity of the member, nonetheless plate imperfections should always be included in the numerical simulations of such members since their effect are not negligible.

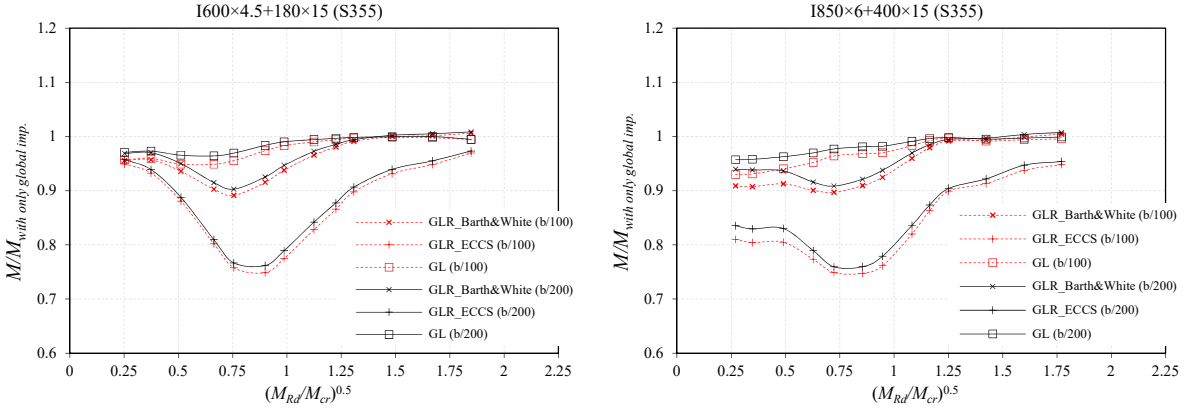

Figure 11: Influence of plate imperfections on the I600×4.5+180×15 (left) and I850×6+400×15 (right) sections.

In addition, the effect of different shape of plate imperfections is investigated here. Two sections were considered in this part of the study, namely the I850×6+400×15 and I850×6+400×20. Figure 12 shows the first local eigenmodes representative of these two sections but using different web

thicknesses in order to vary the shape of imperfections, thus Case 1 represents the most displaced nodes in the web, Case 2 in the flange. Additionally, a third case, Case 3, was considered with the shape corresponding to the summation of Case 1, but with the displacements of flange nodes set to zero, and Case 2, but with the displacements of web nodes set to zero. For the amplitude of the plate imperfections, in both cases 1 and 2 the value of $h_w/100$ was used, for the third case, the imperfection on the web plate is scaled to $h_w/100$ and to $b_f/100$ on the flanges.

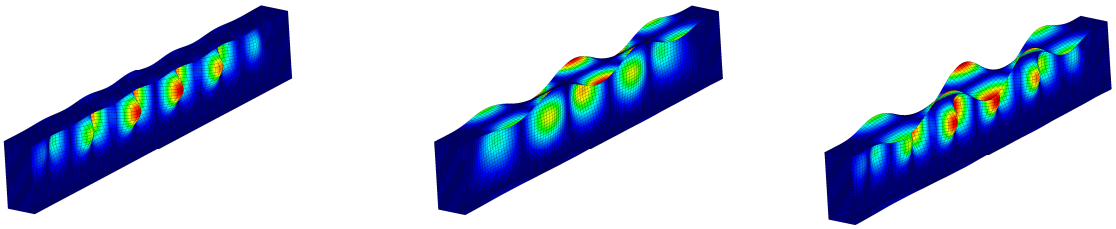

Case 1 (t_w = 6 mm) Case 2 (t_w = 10 mm) Case 3 (≈ Case 1 + Case 2)

Figure 12: Shape of different local imperfections considered.

The influence of using these alternative shapes in the numerical simulations is not negligible, as it can be seen on Figure 13, if the same amplitude for the most displaced node is used, here it was considered as h_w/100. For example, regarding the shortest length, where such influence is higher, around 8% less resistance is obtained when Case 2 is considered as opposed to the first local buckling mode returned from LBA and herein represented by Case 1 for the I850×6+400×15 cross-section. However, this is unrealistic since the flange imperfections is excessive and it is evident that a beam with such imperfections should be rejected from the production point of view. For Case 3, however, realistic imperfections are used and it is demonstrated that differences in the results exist, and are not necessarily negligible. In any case, because this imperfections affect only the shortest lengths where the section capacity governs the load-carrying capacity and the failure mode is not governed by the lateral-torsional buckling, it is considered that a 3-4% difference is acceptable on the results, and, on the remaining study, LBA imperfections based on the shape of the first local eigenmode are used.

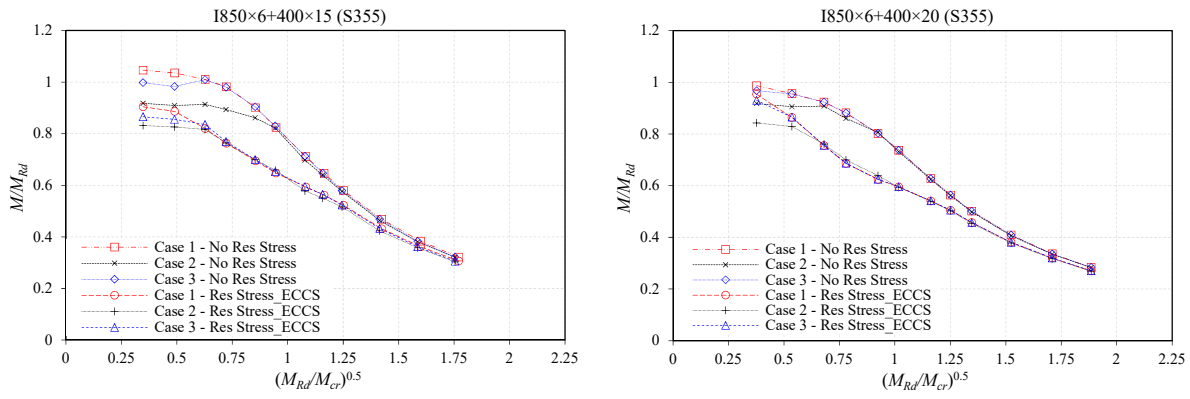

Figure 13: Results for I850×6+400×15 (left) and I850×6+400×20 (right) section with different cases for plate imperfections.

6. Thickness of flange and the effective section factor

The flange determines the capacity of a girder and a variation in the thickness has different consequences in the load-carrying capacity of a girder with slender cross-section. To analyze this influence, the imperfections are maximized (L/1000 as global imperfection and b/100 as plate imperfections) and the residual stresses assumed to have the most detrimental distribution, which corresponds to the "ECCS" pattern. First, it is clear that, due to the presence of such plate imperfections and/or residual stresses the cross-section elastic capacity ($M_{el,y}$ or M_{yc} in the EC3 or AISC360-16 notation, respectively) is not reached leading to the onset of local buckling and capacity reduction in the "plastic" (or plateau) and inelastic ranges, as shown in Figure 14a, despite the classification of the flange. For example, in this figure, a girder with a compact flange of 15 mm, is only able to reach about 94% of the elastic resistance in the plateau range and for a slender flange of 5 mm the drop is steeper and less than 70% of the elastic capacity is reached. Moreover, for this section with a flange thickness of 5 mm, the results portrayed in Figure 14a show an odd behavior compared to its counterparts. Noticeable this section does not fulfill the proportion criteria recommended in AASHTO (2016) and the flange is classified as Class 4 according to Eurocode 3. Although more studies, for such particular cases, should be envisaged, for the moment it is recommended that such sections are avoided in structural solutions where LTB is expected to be the relevant limit state.

To account with the local buckling, the Eurocode 3 proposes the use of a reduced cross-section, calculated based on the effective width method available in Part 1-5, and then the design curves are the same as the ones used for the other sections where local buckling is not determinant. This method, however, does not properly account with the web-flange interaction since it is based on simply supported plate's assumption, and might overestimate the section capacity on the plateau range for more slender sections (see the cases with thicknesses smaller than 10 mm on Figure 14b). On the other hand, it is known that the presence of residual stresses for sections in compression leads to overestimation of the capacity when the effective width expressions of EC3-1-5 are used as noted by different authors (Johansson and Veljkovic, 2009; Schillo, Taras and Feldmann, 2018; Couto and Vila Real, 2019), and there is no reason why it should be different for sections subjected to bending.

The AISC360-16 includes the Flange Local Buckling limit state and the factor R_{pg} which, to a certain extent, allows to account with the effects of local buckling and the interaction between the web and the flange, see Figure 1.

Finally, to consider the proper reduction in the cross-sectional capacity due to local buckling, a FEM analysis of a structural member with a length of ten times the web height and discrete bracing along its lengths to ensure that LTB is not a failure mode is simulated. For these simulations the global imperfections are disregarded and the obtained ultimate strength corresponds to the cross-sectional capacity (or flexure strength), this case is denoted as $M_{Rd} = M_{FEM.}$

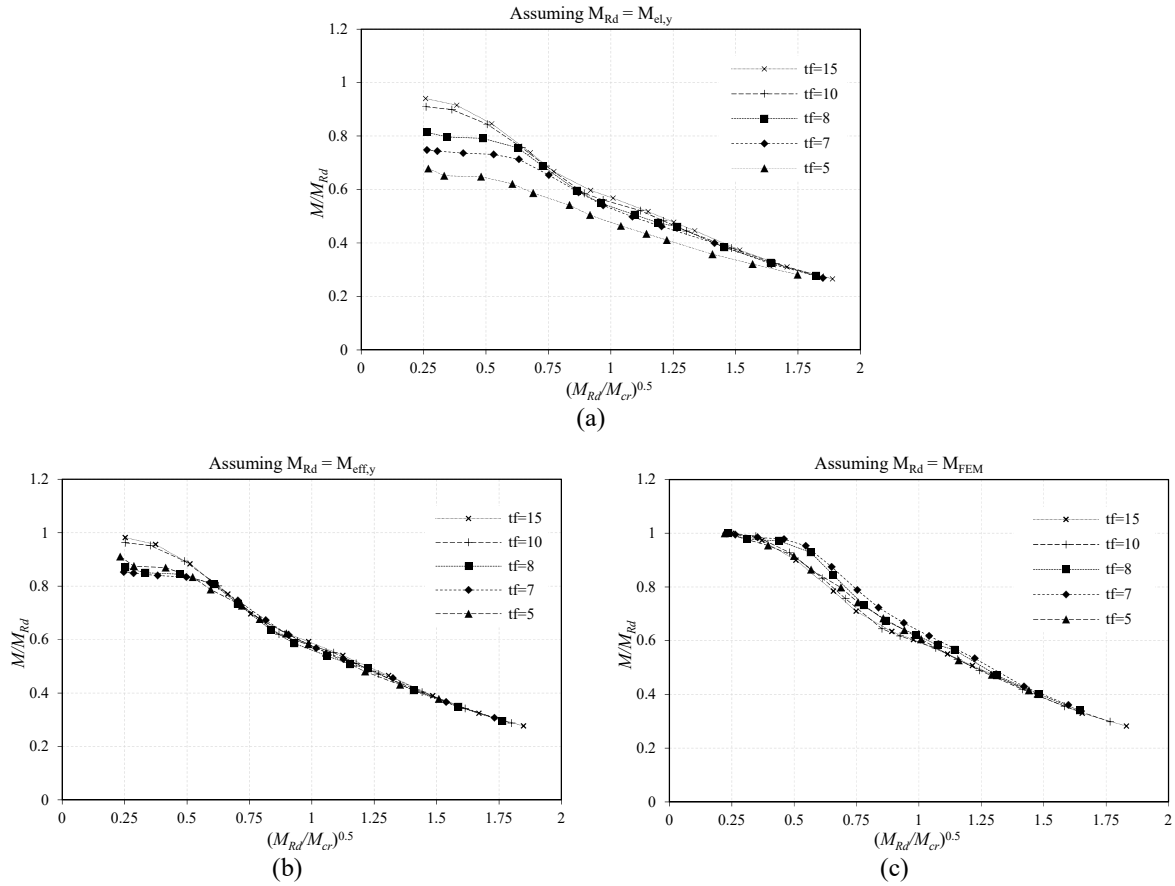

Figure 14: Buckling curve representation of sections I600×4.5+180×tf (S355) assuming cross-section resistance calculated with (a) elastic flexural resistance, (b) the effective width method of EC3-1-5 and (c) from FEM.

If either the elastic cross-section resistance or the effective width expressions given in the present version of EC3-1-5 are used, results are scattered at the lower slenderness range up to 0.75, for instance. In this region the response of the girder is expected to be governed by the capacity of the cross-section rather than the lateral-torsional buckling capacity. For slender girders, for instance with a slenderness greater than 1.5, the results are less scattered, suggesting that in this region, because the response of the girder is governed mostly by the lateral-torsional buckling capacity, it is irrelevant whether the elastic or reduced cross-sectional capacity is used for the design curve, provided that the same cross-sectional capacity is used for the calculation of the slenderness of the member in order to be consistent. Notably, in the inelastic region where an interaction between the capacity of the cross-section and the lateral-torsional buckling instability is expected, the results are more scattered when using the elastic cross-sectional capacity instead of the reduced effective counterpart. In this case, the results suggest that this phenomena might not be properly accounted for using these assumptions and it would be preferable to limit the capacity of the cross-section to account with local buckling. Finally, if the flexure capacity of the girder is determined *a priori* for continuously braced supporting conditions and subjected to uniform (and constant) bending moment, this can be assumed as the cross-sectional capacity (hereby denoted as M_{FEM}) for the analyzed case and the plot in Figure 14c can be drawn. This figure shows an interesting particularity regarding the scatter of the results and the reduction in the capacity due to the lateral-

torsional buckling influence on the member response. The cross-section where local buckling is more preeminent, for example the one with 180×7 flange, the corresponding reduction in capacity due to the influence of lateral-torsional buckling is smoother as the slenderness of the member increases when compared to the cross-section where local buckling is less relevant, the one with 180×15 flange. This evidence was exploited for the case of fire (Couto *et al.*, 2016, 2018) to characterize the response of the steel beams with slender cross-sections through the development of an effective section factor and the proposal of different design curves based on it.

7. Results comparison with North American and European design codes

This section portrays the comparison between the numerical results and the North American and European design codes, the AISC360-16 (2016) and the Eurocode 3 (CEN, 2005), respectively. Results are plotted in Figure 15 for the sections Table 2.

In each case, different assumptions in terms of residual stresses and geometrical imperfections were used. For the AISC360-16, 50% of the Best-fit Prawel pattern was used as the residual stresses distribution, a global imperfection of L/2000 and b/200 for the plate imperfections were considered. This is in accordance with similar studies, for instance of Subramanian and White (2017b), moreover the elastic section resistance was used, thus $M_{Rd} = M_{yc}$. For the comparison with the Eurocode 3, the "ECCS" residual stress distribution was used and L/1000 was adopted as global imperfection and for the plate imperfections they were scaled to 80% of the fabrication tolerances given in the EN1090-2:2011 which corresponds to a value generally between b/100 and b/150, see (Couto and Vila Real, 2019), in this comparison the effective section in accordance with Part 1-5 was used as M_{Rd} and buckling curve "d", as defined in Table 1, was considered.

For the purpose of the comparison, it is assumed that the result from the numerical simulation corresponds to the reference result thus if a method predicts higher capacity, then the case is considered unsafe.

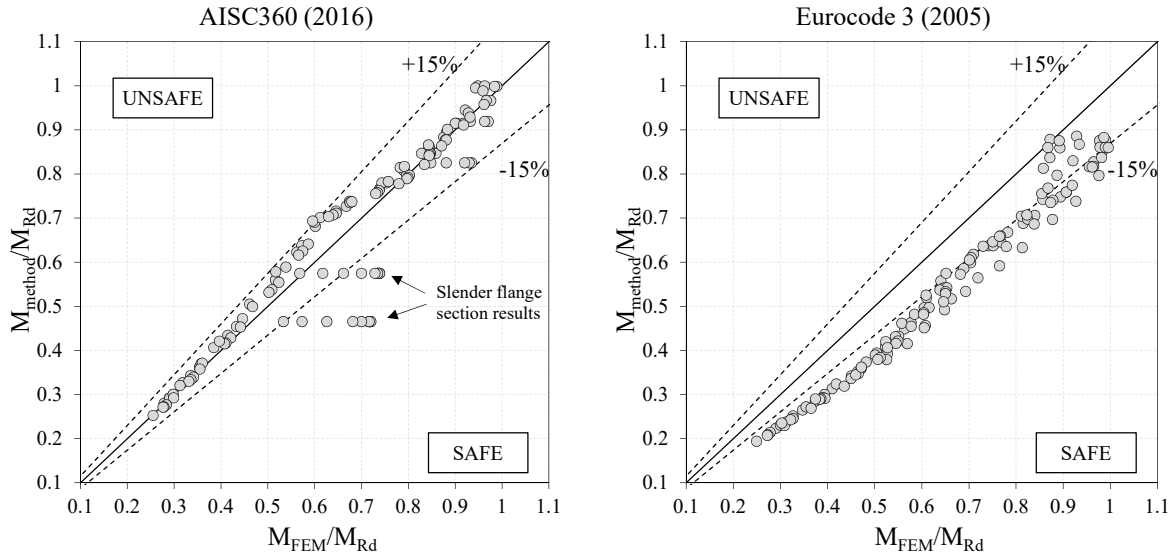

Figure 15: Comparison of FEM results against design codes for different assumptions regarding imperfections and residual stresses.

The comparison shows that the method in AISC360-16 is slightly unsafe, especially in the inelastic region of the design curve as illustrated also in Figure 16. In addition, it is observed that for the cases where the flange is slender according to AISC360-16 classification, results are overly conservative.

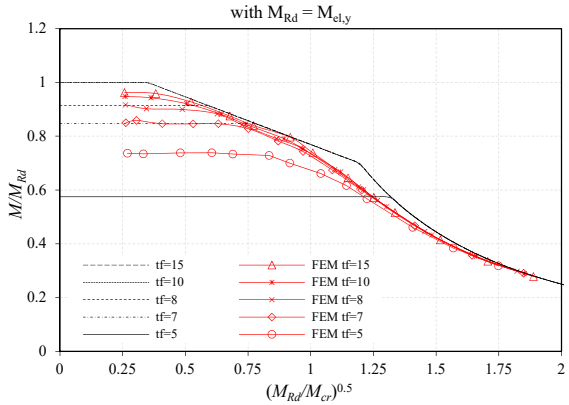

Figure 16: Buckling curve comparison between FEM results and AISC360-16 design curve for I600×4.5+180×tf section.

For the Eurocode 3, the use of buckling curve "d" leads to excessive conservativeness of the design method and it would be recommended to adopt a less severe design curve. In Figure 17 results for all the sections in Table 2 are plotted with the buckling curve representation, where it is shown that buckling curve "c" could be used instead as the design curve.

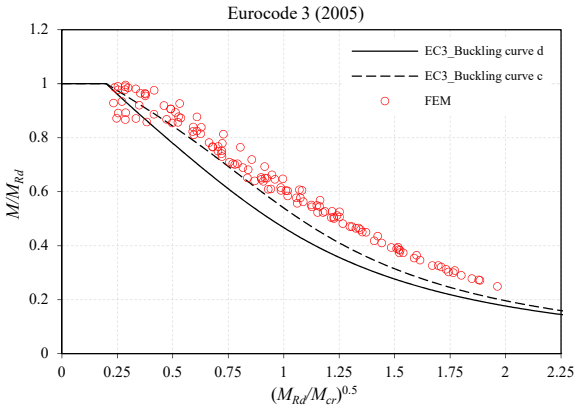

Figure 17: Buckling curve comparison between FEM results and Eurocode 3.

The analysis of the influence of residual stresses and global imperfections on the ultimate strength has shown that considering 50% of the Best-fit Prawel distribution leads to the lowest reduction in the capacity while using the "ECCS" distribution leads to the highest reduction. Thus, both codes seem to be in opposite directions regarding the capacity prediction, with the AISC360-16 code giving an upper bound limit for the resistance and the Eurocode 3 the resistance lower bound.

8. Conclusions

This paper has analyzed the interaction between the local buckling and the lateral-torsional buckling and its influence on the carrying capacity of beams with slender I-shape section. The influence of the plate imperfections, global imperfections and different residual stress patterns was investigated and, as a general rule, using half the Best-fit Prawel residual stress distribution, L/2000 as a global imperfection and b/200 as plate imperfections will lead to an upper bound limit for the beam resistance, and using the ECCS pattern with L/1000 as global imperfection and b/100 will lead to a lower bound limit of the resistance of the beam.

The interaction of local buckling and lateral-torsional buckling was observed to affect the ultimate capacity of the beams. This interaction occurs mainly in the plateau and inelastic range. Furthermore, if a flange is classified as slender according to the AISC360-16, its use should be avoided due to the odd behavior observed, which indicates further studies are needed, despite that, the AISC360-16 design code predicts safe results, although uneconomical for these cases. For the Eurocode 3, if a web is Class 4 and the flange is Class 3 or 4, the code seems not to predict accurately the section resistance, however, this critical behavior is later overcome by adopting a more restrictive design curve for LTB, causing the results to be too much on the safe and uneconomical side for higher girder slenderness.

Finally, from the observations in this paper, it is recommended that the effect of the residual stresses is carefully determined on the basis of experimental tests for future curve calibration. Especially, the determination of the distribution and magnitude is fundamental for the proper characterization of its influence in the ultimate strength of the beams with I-shape slender section. Ultimately, this would clarify whether the AISC360-16 design curve should be reassessed to predict lower values for the resistance or the Eurocode 3 design curves should be recalibrated in order to provide higher capacity predictions of the resistance.

Acknowledgments

This research work was funded by the Portuguese Government through the FCT (Fundação para a Ciência e a Tecnologia) under the Post-doc grant SFRH/BPD/114816/2016 awarded to the first author.

References

AASHTO (2016) *LRFD Bridge Design Specifications*.

AISC (2016) 'Specifications for Structural Steel Buildings', *Chicago*.

Barth, K. E. and White, D. W. (1998) 'Finite element evaluation of pier moment-rotation characteristics in continuous-span steel I Girders', *Engineering Structures*, 20(8), pp. 761–778. doi: 10.1016/S0141-0296(97)00087-4.

Basler, K. and Thürlimann, B. (1960) *Strength of plate girders in bending*. Lehigh University, Fritz Engineering Laboratory.

CEA (2015) 'CAST 3M is a research FEM environment; its development is sponsored by the French Atomic Energy Commission <http://www-cast3m.cea.fr/>.'

CEN (2005) 'EN 1993-1-1, Eurocode 3: Design of steel structures - Part 1-1: General rules and rules for buildings'. Brussels: European Committee for Standardisation.

CEN (2006) 'EN 1993-1-5, Eurocode 3 - Design of steel structures - Part 1-5: Plated structural elements'. Brussels: European Committee for Standardisation, pp. 1–53.

Chacón, R., Mirambell, E. and Real, E. (2009) 'Influence of designer-assumed initial conditions on the numerical modelling of steel plate girders subjected to patch loading', *Thin-Walled Structures*, 47(4), pp. 391–402. doi: 10.1016/j.tws.2008.09.001.

Chacón, R., Serrat, M. and Real, E. (2012) 'The influence of structural imperfections on the resistance of plate girders to patch loading', *Thin-Walled Structures*, 53, pp. 15–25. doi: 10.1016/j.tws.2011.12.003.

Clarin, M. (2004) *High strength steel: local buckling and residual stresses*. Lulea University of Technology.

Couto, C. *et al.* (2015) 'Numerical investigation on lateral torsional buckling of steel beams with class 4 cross-sections - comparison with existing design formulae', in *Eighth International Conference on Advances in Steel Structures*. Lisbon, Portugal.
Couto, C. *et al.* (2016) 'Numerical investigation of the lateral–torsional buckling of beams with slender cross sections for the case of fire', *Engineering Structures*. Elsevier Ltd, 106, pp. 410–421. doi: 10.1016/j.engstruct.2015.10.045.
Couto, C. *et al.* (2018) 'The effect of non-uniform bending on the lateral stability of steel beams with slender cross-section at elevated temperatures', *Engineering Structures*, 163, pp. 153–166. doi: 10.1016/j.engstruct.2018.02.033.
Couto, C. and Vila Real, P. (2019) 'Numerical investigation on the influence of imperfections in the local buckling of thin-walled I-shaped sections', *Thin-Walled Structures*. Elsevier Ltd, 135(June 2018), pp. 89–108. doi: 10.1016/j.tws.2018.10.039.
ECCS (2000) *New lateral torsional buckling curves kLT - numerical simulations and design formulae.* Edited by ECCS. European Convention for Constructional Steelwork Technical Committee No. 8.
Franssen, J. and Gernay, T. (2017) 'Modeling structures in fire with SAFIR ®: Theoretical background and capabilities', *Journal of Structural Fire Engineering*, pp. 1–28. doi: 10.1108/JSFE-07-2016-0010.
Johansson, B. and Veljkovic, M. (2009) 'Review of plate buckling rules in EN 1993-1-5', *Steel Construction*, 2(4), pp. 228–234. doi: 10.1002/stco.200910031.
Kim, Y. (2010) *Behavior and design of metal building frames using general prismatic and web-tapered steel I-section members*. Georgia Institute of Technology.
Rebelo, C. *et al.* (2009) 'Statistical evaluation of the lateral–torsional buckling resistance of steel I-beams, Part 1: Variability of the Eurocode 3 resistance model', *Journal of Constructional Steel Research*. Elsevier Ltd, 65(4), pp. 818–831. doi: 10.1016/j.jcsr.2008.07.016.
Schillo, N., Taras, A. and Feldmann, M. (2018) 'Assessing the reliability of local buckling of plates for mild and high strength steels', *Journal of Constructional Steel Research*, 142, pp. 86–98. doi: 10.1016/j.jcsr.2017.12.001.
Simões da Silva, L. *et al.* (2009) 'Statistical evaluation of the lateral–torsional buckling resistance of steel I-beams, Part 2: Variability of steel properties', *Journal of Constructional Steel Research*. Elsevier Ltd, 65(4), pp. 832–849. doi: 10.1016/j.jcsr.2008.07.017.
Subramanian, L. and White, D. W. (2015) 'Evaluation of Lateral Torsional Buckling Resistance Equations in AISC and', *Structural Stability Research Council*, (January), pp. 1–20.
Subramanian, L. and White, D. W. (2017a) 'Improved Noncompact Web-Slenderness Limit for Steel I-Girders', *Journal of Structural Engineering*, 143(4), p. 04016216. doi: 10.1061/(ASCE)ST.1943-541X.0001722.
Subramanian, L. and White, D. W. (2017b) 'Reassessment of the Lateral Torsional Buckling Resistance of I-Section Members: Uniform-Moment Studies', *Journal of Structural Engineering*, 143(3), p. 04016194. doi: 10.1061/(ASCE)ST.1943-541X.0001686.
Subramanian, L. and White, D. W. (2017c) 'Resolving the disconnects between lateral torsional buckling experimental tests, test simulations and design strength equations', *Journal of Constructional Steel Research*. Elsevier Ltd, 128, pp. 321–334. doi: 10.1016/j.jcsr.2016.08.009.
Talamona, D. and Franssen, J.-M. (2005) 'A Quadrangular Shell Finite Element for Concrete and Steel Structures Subjected to Fire', *Journal of Fire Protection Engineering*, 15(4), pp. 237–264. doi: 10.1177/1042391505052769.
Taras, A. (2010) *Contribution to the Development of Consistent Stability Design Rules for Steel Members*. TU Graz.
Taras, A. and Greiner, R. (2010) 'New design curves for lateral–torsional buckling—Proposal based on a consistent derivation', *Journal of Constructional Steel Research*. Elsevier Ltd, 66(5), pp. 648–663. doi: 10.1016/j.jcsr.2010.01.011.